

Original Research

Evaluation of Urban Ecological Environment Quality Based on Google Earth Engine: A Case Study in Xi'an, China

Shuo Yang, Hao Su*

School of Public Administration, Xi'an University of Architecture and Technology, Xi'an, China

Received: 22 February 2022

Accepted: 27 July 2022

Abstract

The rapid expansion of cities has accelerated the impact of human activities on the ecological environment. Existing studies conducted quantitative evaluations of ecological environment quality through complex remote sensing image screening and processing. Dynamic monitoring and modeling based on cloud platform programming are still lacking at present. This paper evaluated the quality of the ecological environment in Xi'an in 2000, 2005, 2010, 2015, and 2020 using the Remote Sensing Ecological Index (RSEI) model. We selected high-quality remote sensing images based on the Google Earth Engine platform (GEE). The calculation of four indicators and the Principal Component Analysis (PCA) were performed on the platform using JavaScript. The geodetector model was used to detect factors affecting the spatial differentiation of RSEI. The results showed that: (1) The ecological environment quality of Xi'an city during 2000-2020 showed a temporal trend of decreasing and then increasing, and a spatial trend of north-low and south-high. The RSEI value for Xi'an was 0.665 in 2000, 0.653 in 2005, 0.623 in 2010, 0.644 in 2015, and 0.651 in 2020. (2) The Bad level and Fair level of RSEI were mainly distributed in the city's built-up area, and RSEI values were better in the Qinling Mountains. From 2000 to 2020, we found the deterioration areas of RSEI mainly distributed in the Weiyang, Baqiao, Yanliang, Chang'an, and Huyi districts. The improvement areas were mainly distributed in the southeastern mountains. (3) From the geodetector results, elevation (DEM), slope (SLO), precipitation (PRE), temperature (TEM), distance to main roads (ROA), distance to settlements (SET), land use/land cover (LUC), GDP, and population (POP) significantly influenced the regional RSEI spatial differentiation. The rankings of the explanatory power of the single factors were mainly: PRE>TEM>DEM> ROA>LUC>SLO>GDP> SET>POP. PRE has the strongest explanatory power of the nine factors. (4) Positive spatial auto correlation existed for the RSEI values in Xi'an. The Moran's I was 0.513 in 2000, 0.659 in 2005, 0.749 in 2010, 0.716 in 2015, and 0.631 in 2020, respectively. The Local Moran's I of RSEI values showed

*e-mail: suhao@xauat.edu.cn

H-H and L-L clustering. This study provides significant information to identify ecologically fragile urban areas and support ecological environment policymaking.

Keywords: ecological quality, remote sensing ecological index (RSEI), Google Earth Engine, geodetector, Xi'an

Introduction

Ecological environment quality comprehensively represents ecosystem elements, structure, and function in a specific time and space [1]. An excellent ecological environment background plays a critical role in achieving regional sustainable social and economic development [2]. With increasing human activities, urbanization brings inevitable adverse effects such as "urban ecological degradation" [3]. The contradiction between population, resources, and environment is becoming more and more prominent, and the construction of ecological cities has become a hot topic of discussion in today's society [4]. As an emerging concept, building an ecological city has gradually become a hot topic in the urban planning field [5]. With the accelerated urbanization, not only the ecological environment quality inside the urban area degraded, but also the cropland quality around the urban area declined, the productivity of the vegetation reduced, and the phenomenon of land salinization even occurred [6-8]. Assessing the quality of the urban ecological environment, understanding the ecological environment condition, and grasping its change law help promote the sustainable development of the regional economy and have important practical significance and reference value for the construction of urban ecological civilization [9].

There are two commonly used methods for monitoring and evaluating ecological environment quality, the single indicator method and the multiple indicator method. The single indicator method focuses on constructing indices responding to one particular aspect of the ecosystem. The Normalized Difference Vegetation Index (NDVI), the Leaf Area Index (LAI) and the Enhanced Vegetation Index (EVI) are used to reflect vegetation cover changes in ecological studies [10-12]. The land surface temperature (LST) metric is used for surface temperature inversion and can measure the urban heat island effect [13]. Remote sensing technologies can also evaluate water quality, atmosphere pollution, etc. [14, 15]. For more complex study areas, the impact of multiple indicators needs to be considered comprehensively. Scholars should consider the comprehensive effects of multiple indicators' impact in complex environments. The Chinese State Environmental Protection Administration proposed the Ecological Environment Index (EI) that couples the biological richness index, environmental index, water network density index, vegetation cover index, and land degradation index [16]. The statistical data in the multi-indicator evaluation methods are challenging to obtain,

and the index weights are disturbed by human factors, which has certain limitations [17].

Remote Sensing Ecological Index (RSEI) is a regional ecological environment evaluation index proposed by Xu et al. based on remote sensing technology [17]. The construction of this index integrates four remote sensing ecological indexes of greenness, humidity, dryness, and heat [18]. The RSEI excludes the influence of subjective factors and makes up better for the shortcomings of research methods such as the EI, fuzzy assessment method, and comprehensive index [19]. Researchers widely used the RSEI model to evaluate the ecological status of different regions such as cities, deserts, wetlands, river and lake basins, nature reserves, minings, soil erosion areas, etc. [20-27]. RSEI can reveal the ecological environment status between regions, which makes up for the previous single-time section study's shortage and helps quantify and understand the regional ecological environment more deeply. Therefore, it provides a more intuitive decision basis for guiding the region to improve the ecological environment and perform ecological functions [28]. The traditional method requires a personal computer to preprocess the remote sensing images for atmospheric correction, radiometric correction, and seamless mosaic before use. When the study area is large, with many bad pixels, such as clouds, researchers will waste much time on the preliminary preparation. The Google Earth Engine platform provides an extensive archive of historical remote sensing data and cloud computing services, based on JavaScript language programming, making research on large-scale scales possible [29]. The GEE platform has been used to detect the dynamic changes of RSEI in highly geohazard susceptible zones, mountain ranges, river basins, and urban agglomerations [30-34]. Our research used JavaScript language to process the data on the cloud server, saving much time than using, e.g., ENVI software. Besides, the approach is easy to generalize. When using the Landsat series' data, scholars can well solve the problems of large cloud volume and wide range in the study area.

Xi'an is an important central city in western China and an essential base for scientific research, education, and industry. Since the Western Development Strategy in 2000 and officially becoming a national central city in 2018, the economic development of Xi'an has produced dramatic changes and a vast expansion of the city's form. Xi'an is located in the northwest inland ecologically fragile area [35]. The study of regional ecological environment quality changes is essential for identifying urban ecological security patterns, local and regional ecological management, and policy

formulation. Yue et al. studied the ecological quality changes of 35 Chinese cities from 1990 to 2015 using RSEI and identified Xi'an as a city with declining ecological quality [36]. However, the remote sensing images they selected was imaged in November, when the vegetation cover in Xi'an was not the maximum, which would affect the NDVI worthy weights. Besides, the surface temperature inversion could not accurately reflect summer's urban heat island phenomenon. Zhu et al. constructed an integrated ecological index using remote sensing images of Xi'an from 1992 to 2014 to explore the effects of the soil adjusted vegetation index (SAVI), the normalized difference moisture index (NDMI), the normalized difference soil index (NDSI), and the normalized difference built-up index (NDBI) on LST. Still, his study did not further explore the mechanism of the spatially divergent effects of the index [37].

This paper processed remote sensing images of Xi'an city from July to September 2000 to 2020 using the Google Earth Engine platform. The authors calculated the RSEI values and area changes and detected the influence of natural and social factors affecting the spatial differentiation of RSEI using the geodetector model. This paper explores a fast measurement of urban ecological environment quality and the influencing factors to provide a basis for regional ecological

environment evaluation and environmental remediation policy formulation.

Material and Methods

Study Area

Xi'an (107.40°E-109.49°E, 33.42°N-34.45°N) is located in the central part of Guanzhong Plain, bordering the Wei River in the north and the Qinling Mountains in the south, with a total area of 10,108 square kilometers. The terrain of Xi'an shows low and flat in the north and mountainous in the south. The plain area of Xi'an is a semi-humid continental monsoon climate of warm temperate zones. The annual average temperature is 13.0-13.7°C, and the annual precipitation is 522.4-719.5 mm. According to the seventh census data, by November 1, 2020, the permanent resident population of Xi'an was 12,952,907. The GDP of Xi'an was 1002.039 billion CNY in 2020. In the Development Plan of Guanzhong Plain Urban Agglomeration, Xi'an is approved by the State Council of China as an important central city in the western region of China. It includes 13 districts (counties), Lianhu, Xincheng, Beilin, Yanta, Weiyang, Baqiao, Yanliang, Gaoling, Chang'an, Lintong, Lantian, Huyi, and Zhouzhi (Fig. 1).

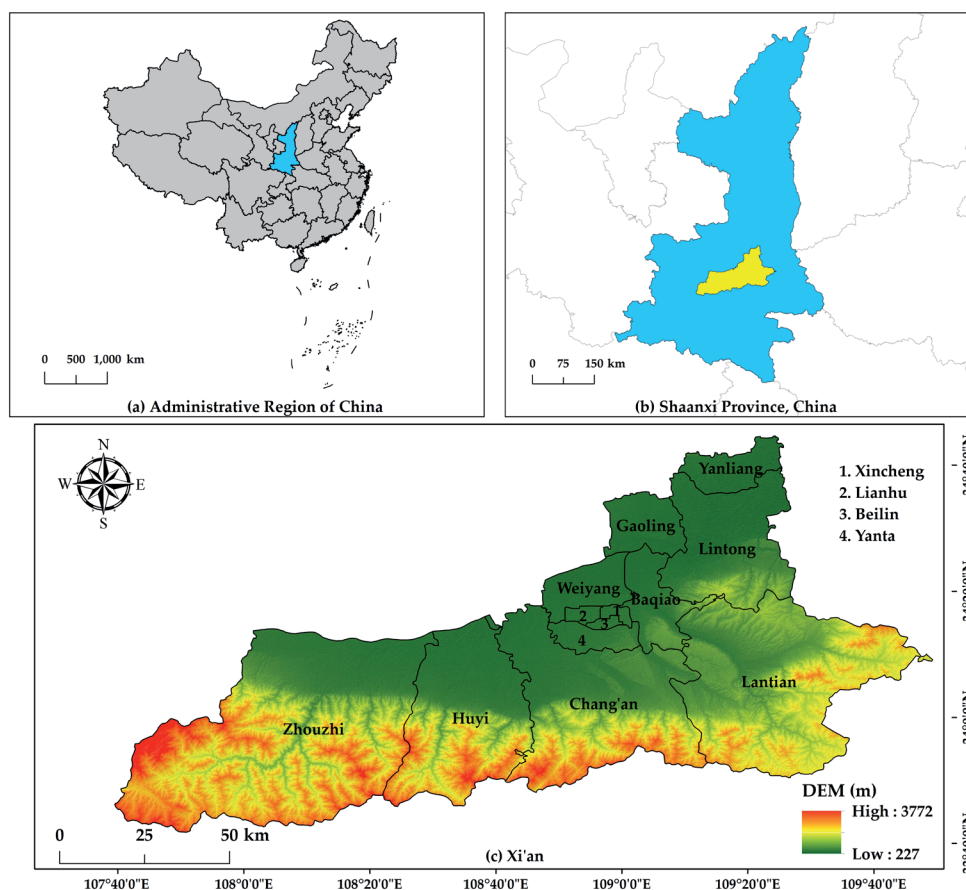


Fig. 1. Study area: Location map of Xi'an, China.

Data and Preprocessing

This study acquired the elevation data from the Geospatial Data Cloud (<http://www.gscloud.cn>) and the administrative divisions' data from the National Basic Geographic Database of the Chinese National Geographic Information Resource Directory Service System (<https://www.webmap.cn>). The land use type data and GDP density raster data were obtained from the Resource and Environment Science and Data Center of the Chinese Academy of Science (<https://www.resdc.cn>). The population density raster data were obtained from the WorldPop project (<https://www.worldpop.org>). In this paper, the "LANDSAT/LT05/C01/T1_SR" datasets of the Landsat 5 TM satellites and the "LANDSAT_LC08_C01_T1_SR" datasets of the Landsat 8 OLI satellites were selected, respectively. The Landsat series surface reflectance (SR) datasets have been geometrically corrected, atmospherically corrected, and radiometrically calibrated, with a spatial resolution of 30 m and a temporal resolution of 16 days. Based on the Quality Assessment (QA) band in the SR datasets provided by the GEE platform, this paper used the "CFMASK" function to remove clouds. The process collects all remote sensing images from July to September in the target year and the year before and after and then replaces the identified bad pixels with transparent sky pixels without cloud coverage. The

MNDWI was used to identify water bodies in the area to reduce the influence of water bodies on the results [38]. The crop growing season around Xi'an city is from July to September, and crop growth strongly influences regional NDVI and NDBSI. Among the years selected, there were many clouds in remote sensing images of this period in 2000, 2005, 2010, 2015, and 2020. Contemporaneous images of neighboring years (the previous and the following year) were chosen and performed median processing to fill the gaps [39].

Remote Sensing Ecological Index Model

RSEI Metrics Extraction

The Remote Sensing Ecological Index (RSEI) model is based on remote sensing information [28]. The model is established considering the vegetation growth state, soil moisture, soil dryness, building land condition, and surface temperature. Normalized Difference Vegetation Index (NDVI) is selected as the greenness index, and Wetness (WET) is selected as the moisture index after tassell hat transformation. Land Surface Temperature (LST) is selected as the heat index, and the Normalized Difference Built-up and Soil Index (NDBSI), the composite result of Soil Index (SI), and Index-based Built-up Index (IBI) are selected as the dryness index (Table 1). The RSEI is expressed as follows [40]:

Table 1. Formula and explanation of four indexes of RSEI model.

Index	Formula	Explanation
NDVI	$NDVI = (\rho_{NIR} - \rho_{Red}) / (\rho_{NIR} + \rho_{Red})$	Where NDVI is taken in the range [-1,1]. ρ_{NIR} is the reflection value in the NIR band, and ρ_{Red} is the reflection value in the red band.
WET	$WET_{TM} = 0.0315\rho_{Blue} + 0.2021\rho_{Green} + 0.3102\rho_{Red} + 0.1594\rho_{NIR}$ $- 0.6806\rho_{SWIR1} - 0.6109\rho_{SWIR2}$ $WET_{OLI} = 0.1511\rho_{Blue} + 0.1973\rho_{Green} + 0.3283\rho_{Red} + 0.3407\rho_{NIR}$ $- 0.7117\rho_{SWIR1} - 0.4559\rho_{SWIR2}$	Where ρ_{Blue} , ρ_{Green} , ρ_{Red} , ρ_{NIR} , ρ_{SWIR1} , ρ_{SWIR2} denote the blue, green, red, near-infrared, and short-wave infrared 1 and 2 bands, respectively [41, 42].
LST	$LST = \frac{T_{sensor}}{[1 + (\lambda \times \frac{T_{sensor}}{\rho}) \ln \epsilon]}$ $\epsilon = \begin{cases} 0.995 & (NDVI \leq 0) \\ 0.970 & (0 < NDVI \leq 0.157) \\ 0.986 & (NDVI > 0.727) \\ 1.0094 + 0.047 \ln NDVI & (0.157 < NDVI \leq 0.727) \end{cases}$ $T_{sensor} = \frac{K_2}{\ln(\frac{K_1}{L_\lambda} + 1)}$ $L_\lambda = Gain \times DN + Bias$	Where λ is the wavelength of the emitted radiance (11.435 μ m for band 6 of Landsat 5 and 10.9 μ m for band 10 of Landsat 8); ρ is a constant (1.438 $\times 10^{-2}$ m K); ϵ is the land surface emissivity [43, 44]; T_{sensor} is the at-satellite brightness temperature in Kelvin; L_λ is the at-sensor spectral radiance; Gain and Bias are the band gain and offset values, respectively; DN represents the digital number of a given pixel; K_1 and K_2 are calibration parameters [36, 45].
NDBSI	$IBI = \frac{2\rho_{SWIR1}(\rho_{SWIR1} + \rho_{NIR})^{-1} - \rho_{NIR}(\rho_{Red} + \rho_{NIR})^{-1} - \rho_{Green}(\rho_{SWIR1} + \rho_{Green})^{-1}}{2\rho_{SWIR1}(\rho_{SWIR1} + \rho_{NIR})^{-1} + \rho_{NIR}(\rho_{Red} + \rho_{NIR})^{-1} + \rho_{Green}(\rho_{SWIR1} + \rho_{Green})^{-1}}$ $SI = \frac{[(\rho_{SWIR1} + \rho_{Red}) - (\rho_{NIR} + \rho_{Blue})]}{[(\rho_{SWIR1} + \rho_{Red}) + (\rho_{NIR} + \rho_{Blue})]}$ $NDBSI = (IBI + SI) / 2$	Where SI and IBI represent Soil Index and Building Index, respectively [28].

$$RSEI=f(NDVI,WET,LST,NDBSI) \quad (1)$$

where NDVI, WET, LST, NDBSI represent the greenness, wetness, heat, and dryness, respectively.

Comprehensive Index Construction

Principal Component Analysis (PCA) can transform multiple variables into a few crucial variables by a linear transformation, eliminate redundant information, and obtain a comprehensive index that concentrates most of the characteristics of the original index. Each index measure unit is not unified and needs to be normalized by the formula as follows:

$$NI_i = \frac{I_i - I_{\min}}{I_{\max} - I_{\min}} \quad (2)$$

where NI_i is the normalized index value in the range of [0, 1], I_i is the index value at pixel i , and I_{\max} and I_{\min} are the maximum and minimum values of the index, respectively.

Principal component calculations of RSEI indicators were performed using the normalized indicators, and the results were similarly normalized as follows:

$$RSEI = \frac{RSEI_0 - RSEI_{0_min}}{RSEI_{0_max} - RSEI_{0_min}} \quad (3)$$

where larger value stands for better ecological environment quality condition, and con-versely, the lower, the worse.

Geodetector Model

Geodetector can detect whether a particular factor effectively affects the spatial distribution of a specific type of indicator, including four types of detectors: factor detector, interaction detector, risk detector, and ecological detector [46]. Geodetector was widely used in the evaluation of spatial variation in ecological quality [47, 48]. In this paper, the authors introduced the factor detector to explore the influence mechanism of the spatial distribution of each influencing factor. It is used to detect the spatial heterogeneity of remote sensing indices, i.e., the degree of influence of a particular factor X on the spatial heterogeneity of each remote sensing index Y in the RSEI model. The q value measures the influence degree, and the larger the q value is, the more noticeable the influence of X on the spatial heterogeneity of Y, which can be expressed as:

$$q = 1 - \frac{1}{n\sigma^2} \sum_{h=1}^L N_h \sigma_h^2 = 1 - \frac{SSW}{SST} \quad (4)$$

where $h = 1, \dots, L$ is the stratification of the ecological index value influence factor, N_h and N are the number

of cells in stratum h and the whole area, respectively; σ_h^2 and σ^2 are the variances of Y value in stratum h and the whole area, respectively; SSW, SST are the sum of variance within a stratum and the total variance of the whole area, respectively. Suppose the independent variable X generates the stratification. In that case, the larger value of q indicates the stronger explanatory power of factor X on Y; on the contrary, the power is weaker [49].

Spatial Autocorrelation Analysis

Spatial auto-correlation is an vital indicator for testing the correlated significance of attribute value of an ecological index with the attribute value of its adjacent space [50]. The Global Moran's I (Moran's I) index reflects the correlation of attribute values of adjacent spatial units [51]. The Global Moran's I can be calculated as follows [52]:

$$\text{Global Moran's I} = \frac{N \sum_i \sum_{ij} w_{ij} (x_i - \bar{x})(x_j - \bar{x})}{(\sum_i \sum_{ij} w_{ij}) \sum_i (x_i - \bar{x})^2} \quad (5)$$

where w_{ij} , x_i , x_j , μ and N indicate the normalized weights, RSEI value in the i_{th} pixel, RSEI value in the j_{th} pixel, mean RSEI value of the study area, and the total number of pixels, respectively.

Local Moran's I (LISA) index can effectively reflect the correlation between the ecological environment quality of each grid unit in the study area [53]. The calculation formula is as follows:

$$\text{Local Moran's I} = \frac{(x_i - \bar{x}) \sum_{ij} w_{ij} (x_j - \bar{x})}{\sum_i (x_i - \bar{x})^2} \quad (6)$$

where the calculation parameters are the same as the Moran's I index. LISA cluster map has five types of local spatial aggregation, namely High-High (H-H), Low-Low (L-L), Low-High (L-H), High-Low (H-L), and No Significant.

Results and Discussion

PCA Results of the Four Indicators

Table 2 shows the results of the principal component analysis of four indicators in Xi'an. The contribution rates of PC1 in the five years were 77.76%, 83.04%, 79.86%, 90.81%, and 88.25%, respectively, indicating that the PC1 concentrated most of the information of the four indicators: NDVI, WET, LST, and NDBSI. The eigenvectors of NDVI and WET were positive, and the eigenvectors of LST and NDBSI were negative. This result is consistent with objective facts and other studies. In 2000 and 2010, the absolute value of the eigenvector of NDVI was the highest, and the eigenvector of NDBSI followed. In 2005, 2015,

Table 2. Principal component analysis indexes of RSEI.

Year	Indicator	PC1	PC2	PC3	PC4
2000	NDVI	0.566	-0.077	-0.641	-0.513
	WET	0.408	-0.224	0.756	-0.461
	LST	-0.444	-0.865	-0.134	-0.193
	NDBSI	-0.562	0.444	0.009	-0.698
	Eigenvalue	0.150	0.024	0.017	0.002
	Contribution rate	77.76%	12.38%	8.80%	1.07%
2005	NDVI	0.566	0.506	-0.360	0.542
	WET	0.388	-0.764	0.232	0.461
	LST	-0.454	-0.322	-0.793	0.248
	NDBSI	-0.568	0.240	0.433	0.657
	Eigenvalue	0.165	0.022	0.009	0.002
	Contribution rate	83.04%	11.31%	4.68%	0.97%
2010	NDVI	0.592	0.512	-0.423	0.457
	WET	0.319	-0.758	0.130	0.554
	LST	-0.507	-0.233	-0.814	0.164
	NDBSI	-0.539	0.332	0.377	0.676
	Eigenvalue	0.182	0.030	0.013	0.003
	Contribution rate	79.86%	13.20%	5.69%	1.26%
2015	NDVI	0.545	0.112	-0.707	-0.436
	WET	0.432	-0.568	0.528	-0.461
	LST	-0.434	-0.772	-0.465	0.012
	NDBSI	-0.573	0.263	0.077	-0.773
	Eigenvalue	0.235	0.015	0.008	0.001
	Contribution rate	90.81%	5.80%	3.11%	0.28%
2020	NDVI	0.514	0.230	-0.593	0.576
	WET	0.382	-0.522	0.594	0.478
	LST	-0.409	-0.746	-0.507	0.142
	NDBSI	-0.650	0.344	0.200	0.648
	Eigenvalue	0.255	0.023	0.009	0.002
	Contribution rate	88.25%	8.02%	3.16%	0.57%

and 2020, the absolute value of the eigenvector of NDBSI rose to the highest. The absolute value of the eigenvector of WET remains the lowest, and the absolute value of LST remains the third place for five years. The NDVI and NDBSI affected the RSEI value the most of the four indicators.

As the average RSEI value is 0.647 for the periods, Xi'an's ecological environment remains suitable for 20 years. According to the average value of RSEI, the ecological quality of Xi'an showed a trend of decreasing and then increasing. The RSEI value was 0.665 for the year 2000, and the RSEI value dropped to 0.653 in

2005, and the lowest, 0.623 in 2010, with a reduction of 6.32%. The continued decrease remained until 2010; the RSEI value in 2015 rose to 0.644, and the RSEI value in 2020 was 0.651, the highest in the recent ten years. Table 4 shows the average values of four indicators of RSEI. From 2000 to 2010, the average value of NDVI decreased from 0.680 to 0.635, which shows the most significant decline of the four indicators, and in 2015, the NDVI value rose to 0.698, with an increase of 9.92%. The NDVI value remained almost constant in 2020. The average value of WET decreased slightly in 2005, reduced by 0.007, and rose to its highest, 0.699,

Table 3. Average value of RSEI indicators.

Year	NDVI	WET	LST	NDBSI	RSEI
2000	0.680	0.633	0.499	0.360	0.665
2005	0.658	0.626	0.503	0.354	0.653
2010	0.635	0.657	0.475	0.382	0.623
2015	0.698	0.699	0.469	0.379	0.644
2020	0.698	0.680	0.483	0.349	0.651

in 2015. The average value of LST and NDBSI both showed a decreasing trend followed by an increasing trend from 2000 to 2020. The highest average value of LST was 0.503 in 2005, and the highest NDBSI value was 0.382 in 2010.

Spatial Distribution of RSEI in Xi'an

Overall Evaluation of Ecological Environment Quality of Xi'an

According to Xu's research, we classified the RSEI value into five levels: Bad (0-0.2), Fair (0.2-0.4), Moderate (0.4-0.6), Good (0.6-0.8), and Excellent (0.8-1). Table 5 shows the proportion of each grade of RSEI in 2000, 2005, 2010, 2015, and 2020, respectively. The Good and Excellent level area covered more than 50 percent of the total land area. The area of Bad level of RSEI continuously increased from 2000 to 2020. In 2000, the Bad level area covered 597.20 km², and the number rose to 1081.30 km² in 2020. The area of Fair level was 1597.68 km² in 2010 and thus causing the lowest RSEI value. The area of Moderate was the smallest of the twenty years in 2015, while the Good level area decreased by 58.09 km² compared to 2010. The Excellent level area showed an upward trend, rising from 3518.87 km² in 2000 to 4480.71 km² in 2020.

Fig. 2 shows the spatial distribution of RSEI values in Xi'an from 2000 to 2020. In 2000, the Bad level and Fair level of RSEI were mainly in the city's built-up area and the hills in Lintong District and Lantian County next to the urban area. The ecological quality of the Qinling Mountains in the south was quite good.

A large amount of cultivated land surrounds the central metropolitan area of Xi'an and contributes a lot to the good ecological quality. In 2000, the area of Bad level only covered 6.07% of the total area, and the number increased rapidly as fast as the urbanization of Xi'an in the past decades. In 2005, the proportion of Bad levels increased to 7.05% of the total area. A sharp decline in the RSEI level occurred in the Weiyang and Gaoling Districts, two districts on the northwest side of Xi'an's main urban area, next to Xianyang City. The RSEI in Yanliang District also decreased because of the expansion of the impervious surface area. In 2010, the Bad level area reached 9.12%, and the Moderate level and Good level decreased to 15.58%, 16.84%, and 20.18%, respectively. The Fair level area's proportion reached 15.58%, the highest of the five years. The area of Bad level area in 2020 was 193.88km² larger than in 2015, with an increase of 1.8%. The area of Fair and moderate slightly decreased by 1.06% and 1.87%, respectively. The Excellent level area increased by 402.12 km² from 2015 to 2020, and the proportion rose to 44.51%.

Dynamic Changes of RSEI in Xi'an from 2000 to 2020

As mentioned above, the RSEI images of 2000, 2005, 2010, 2015, and 2020 were reclassified into five levels. By overlapping and subtracting the RSEI level maps after reclassification, we can obtain the change levels of RSEI between different years as +4, +3, +2, +1, 0, -1, -2, -3, and -4 (Fig. 3). The five categories of RSEI changing levels were recognized as Obvious

Table 4. The proportion of each grade of urban ecological environment quality of Xi'an.

RSEI Level	2000		2005		2010		2015		2020	
	Area (km ²)	Pct. (%)								
Bad/(0-0.2)	611.42	6.07	708.58	7.05	918.98	9.12	914.34	9.21	1108.22	11.01
Fair/(0.2-0.4)	951.63	9.45	1013.85	10.08	1597.68	15.58	1345.83	13.56	1258.24	12.50
Moderate/(0.4-0.6)	1621.89	16.10	1729.07	17.20	1696.68	16.84	1607.95	16.20	1442.68	14.33
Good/(0.6-0.8)	3392.75	33.68	3114.15	30.97	2033.99	20.18	1975.90	19.91	1777.86	17.66
Excellent/(0.8-0.1)	3495.42	34.70	3488.33	34.70	3829.76	38.00	4079.50	41.11	4481.62	44.51

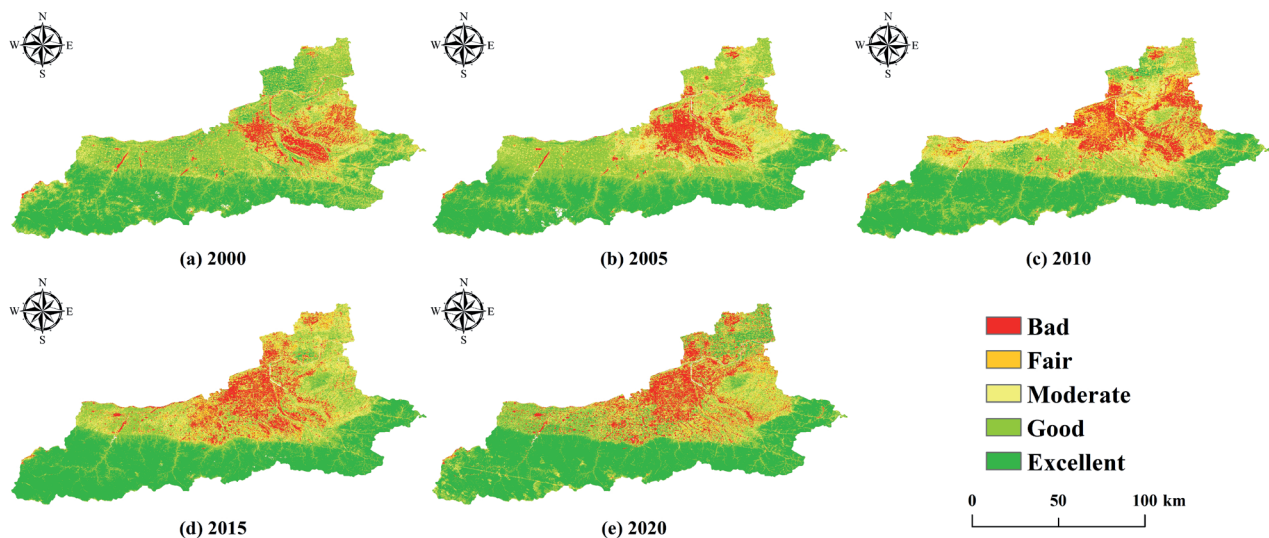


Fig. 2. Spatial distribution of RSEI values in Xi'an from 2000 to 2020.

Improvement (+4, +3), Slight Improvement (+2, +1), Constant (0), Slight Deterioration (-1, -2), and Obvious Deterioration (-3, -4). Table 5 showed the details of reclassification. we divided the overall RSEI changes into nine levels. The five categories of RSEI changing levels were recognized as Obvious Improvement (OI), Slight Improvement (SI), Constant, Slight Deterioration (SD), and Obvious Deterioration (OD). Table 5 shows the statistics of area and proportion changes in RSEI levels.

From 2000 to 2020, the urban ecological pattern of Xi'an changed dramatically (Fig. 3). The Deterioration level area from 2000 to 2010 was mainly distributed around the urban area of Xi'an. The main area of Xi'an expanded to the north and west during this decade. In 2006, the Xi'an city government moved from Lianhu District to the Weiyang District, which led to rapid urbanization in the northwestern part of the city. Many Deterioration level areas were located in the northwest corner of the city. Besides, Improvement level areas

Table 5. Area and proportion changes of RSEI levels from 2000 to 2020.

Year		Obvious Improvement		Slight Improvement		Constant	Slight Deterioration		Obvious Deterioration	
		+4	+3	+2	+1		-1	-2	-3	-4
2000 to 2005	Area/ km ²	0.25	20.03	267.77	1777.70	5681.31	1797.52	355.29	110.20	17.40
	Change area/ km ²	20.28		2045.47		5681.31	2152.81		127.60	
	Percentage/ %	0.20		20.40		56.66	21.47		1.27	
2005 to 2010	Area/ km ²	0.33	7.96	92.80	1422.14	6102.42	1837.78	476.21	93.31	3.99
	Change area/ km ²	8.29		1514.94		6102.42	2313.99		97.31	
	Percentage/ %	0.08		15.09		60.80	23.05		0.97	
2010 to 2015	Area/ km ²	1.62	45.12	416.88	2040.28	5909.72	1141.6	390.38	105.21	5.62
	Change area/ km ²	46.74		2457.15		5909.72	1531.55		110.84	
	Percentage/ %	0.46		24.43		58.77	15.23		1.10	
2015 to 2020	Area/ km ²	5.89	71.29	333.04	1501.61	6367.09	1444.16	280.86	47.82	2.35
	Change area/ km ²	77.18		1834.66		6367.09	1725.02		50.17	
	Percentage/ %	0.77		18.25		63.33	17.16		0.50	
2000 to 2020	Area/ km ²	6.84	82.15	497.35	2236.21	4541.69	1420.81	795.65	383.50	77.87
	Change area/ km ²	89.00		2733.56		4541.69	2216.46		461.37	
	Percentage/ %	0.89		27.22		45.23	22.07		4.59	

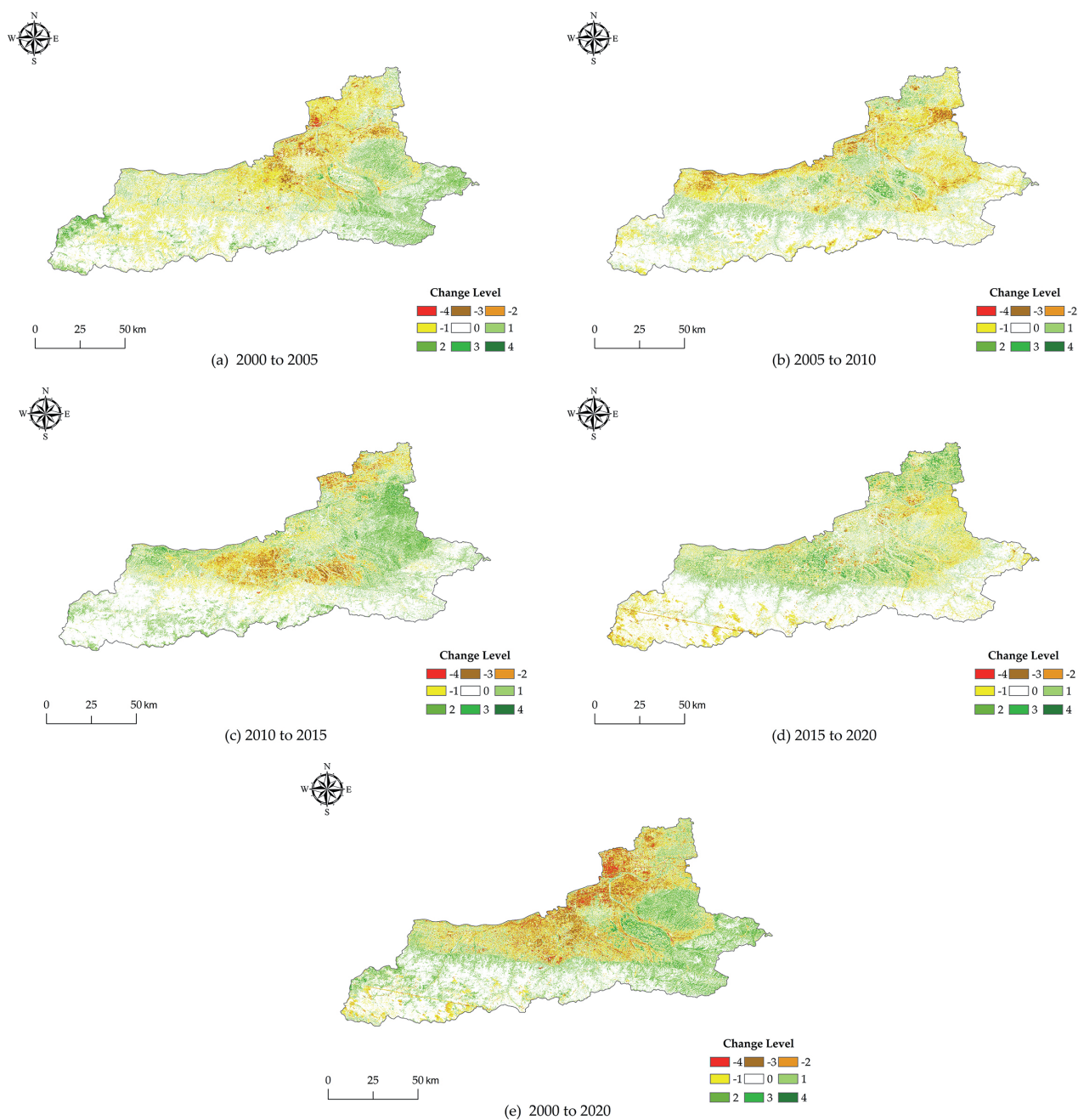


Fig. 3. Change detection of RSEI levels in Xi'an from 2000 to 2020.

were distributed on the city's southeast side. After systematic ecological remediation, the vegetation cover of the area has increased significantly. The RSEI value in this area increased accordingly. From 2010 to 2020, the deterioration level area expansion appeared to be in a southwest and northeast direction. The Northwest part of the urban area stopped expanding because of the saturation of building land. The construction of green space in some areas along the river also resulted in higher RSEI values. With the increase of rural settlements and land for construction, RESI values in Yanliang District and Gaoling District continue to decrease. The Deterioration areas of RSEI were mainly distributed in the north, west, and south directions of

Xi'an urban area, and the Improvement areas were primarily distributed in the southeastern mountains.

Detection and Analysis of Factors Influencing Ecological Environment Quality

Complex human activities and diverse environmental variables influence the changes in RSEI. Topographical factors are key factors affecting the intensity of human activities, and differences in elevation and slope lead to variations in the ecological environment quality [31]. Precipitation and temperature significantly affect the vegetation growth in the region, which directly leads to differences in NDVI values and further affects

the measured RSEI [54]. The spatial differentiation of land use types directly influences the supply of ecosystem services and the expansion of human built-up areas and the construction of roads can significantly affect the regional ecological environment [55]. Accordingly, urban areas with various levels of development have different GDP and population densities, which also affect the spatial differentiation of RSEI [56]. Therefore, in this study, the RSEI in 2020 was selected as the dependent variable, and elevation, slope, average annual precipitation, average annual temperature, distance to main roads, distance to settlements, land use types, GDP, and population density were selected as independent variables concerning existing studies [57-59]. All the nine influencing factors were reclassified using the natural breakpoint method. We used ArcGIS 10.2 to generate a 3 km×3 km grid and sampled 1129 sample points with the center of the grids. In the following, DEM represents the elevation of the region, SLO represents the slope, PRE represents the average annual precipitation, TEM represents the average annual temperature, ROA represents the distance to main roads, SET represents the distance to settlements, LUC represents the land use types, GDP represents the GDP density, and POP represents the population density.

The results of the single factor detection showed that the p values of all the impact factors were zero, which indicated that the influencing factors had significant effects on the spatial differentiation characteristics of RSEI (Table 6). The q-value of PRE remained the highest among other factors, indicating that annual precipitation significantly affects the spatial variation

of RSEI in the region. The q-value of population density was the smallest. Mainly, the rankings were: PRE>TEM>DEM>ROA>LUC>SLO>GDP>SET>POP. The determinants of the interaction results were all higher than the independent determinants of the original 2 factors (Table 7). The spatial heterogeneity of ecological, environmental quality in Xi'an resulted from a single influencing factor and the combined effect of multiple factors interacting and then reinforcing each other. Therefore, all interaction items showed a bilinear enhancement. In terms of the explanatory power of the interactions of the two impact factors, the interactions of PRE ∩ ROA have the strongest explanatory power for the regional RSEI. This demonstrates the effect of the interaction of regional precipitation and distance to roads on the spatial distribution of RSEI. PRE had the strongest explanatory power for the interaction, followed by TEM, DEM, and ROA, in agreement with the single factor detection results.

Spatial Autocorrelation Analysis of RSEI

To study the spatially divergent characteristics of the RSEI values in Xi'an from 2000 to 2020, we used Geoda software to calculate the Global Moran's index and the Local Moran's I index for the study area. We used a 3 km × 3 km grid to resample RSEI images of Xi'an in the five years. We used the default threshold value of 3.17 km in Geoda software as the search radius, generated the distance weight matrices, and performed the spatial autocorrelation analysis. The Local Moran's I and the Global Moran's I have the same spatial weight matrix. The scatterplots of Global Moran's I are shown

Table 6. Results of single factor detector.

Impact factor	DEM	SLO	PRE	TEM	ROA	SET	LUC	GDP	POP
q-Statistic	0.4072	0.2538	0.5001	0.4095	0.3750	0.1848	0.3084	0.2105	0.0807
p-Value	0.0000	0.0000	0.0000	0.0000	0.0000	0.0000	0.0000	0.0000	0.0000
Ranking	3	6	1	2	4	8	5	7	9

Table 7. Detection results of interaction of influencing factors on RSEI.

Factors	DEM	SLO	PRE	TEM	ROA	SET	LUC	GDP	POP
DEM	0.4072								
SLO	0.4619	0.2538							
PRE	0.5290	0.5350	0.5001						
TEM	0.4313	0.4680	0.5277	0.4095					
ROA	0.4656	0.4523	0.5451	0.4615	0.3750				
SET	0.4562	0.3642	0.5379	0.4620	0.4514	0.1848			
LUC	0.4403	0.3812	0.5234	0.4466	0.4429	0.3728	0.3084		
GDP	0.4735	0.3515	0.5429	0.4708	0.4645	0.3393	0.3799	0.2105	
POP	0.4175	0.2871	0.5187	0.4222	0.3915	0.2362	0.3409	0.2329	0.0807

in Fig. 4. Moran's I of these years were all above 0.5 and passed the significance test ($p \leq 0.05$). The Moran's I was 0.513 in 2000, 0.659 in 2005, 0.749 in 2010, 0.716 in 2015, and 0.631 in 2020, respectively, with the highest value in 2010. As shown in the figures, the scatter points are mainly distributed in the first and third quadrants, indicating that the ecological environment quality has a strong positive spatial correlation.

The Local Moran's I were calculated to identify the hot and cold spots of RSEI in Xi'an city. As shown in Fig. 5, the LISA cluster map offers a visual representation of the spatial distribution of the ecological security pattern of Xi'an city. The No Significant area was mainly distributed in the rural area around the central city. In contrast, the H-H clustering area was distributed primarily in the northern part of the city, and the L-L clustering area was distributed in the middle and east. In the L-L clustering area, the terrain is low and flat, and there were large impervious surfaces in the settlements, thus affecting the RSEI of the area. The H-H area was in the Qinling Mountains. The area has high vegetation cover and low human activities, the ecological protection red line area. In 2000, 2005, and 2010, the L-L sample points were distributed in the urban area and the low vegetation-

covered mountains in the east. From 2010 to 2015, the L-L area in Xi'an showed a westward shift in the center. We used the Matlab 2020a to project the sample points to detect the relationship between RSEI and the four indicators of 2020 [60]. The 3D scatterplots are shown in Fig. 6. NDVI and WET contributed positively to RSEI, and LST and NDBSI contributed negatively to RSEI.

Driving Factors of RSEI Changes

RSEI, consisting of NDVI, WET, LST, and NDBSI, is a composite indicator, and its variation mechanism has become a hot spot for scholars [31]. In different study areas, due to the similar driving mechanisms, the trends of regional changes in ecological environment quality were significant due to the impact of human activities. As the regional population density and the impervious surface area grows, the RSEI showed a downward trend in Xiong'an New Area, China [61]. Such findings are consistent with Hang's study, where in Nanjing City, China, the urbanization rate and RSEI evidenced a high negative correlation coefficient value [62]. The common method to examine the influencing factors of RSEI is the use of the correlation coefficient

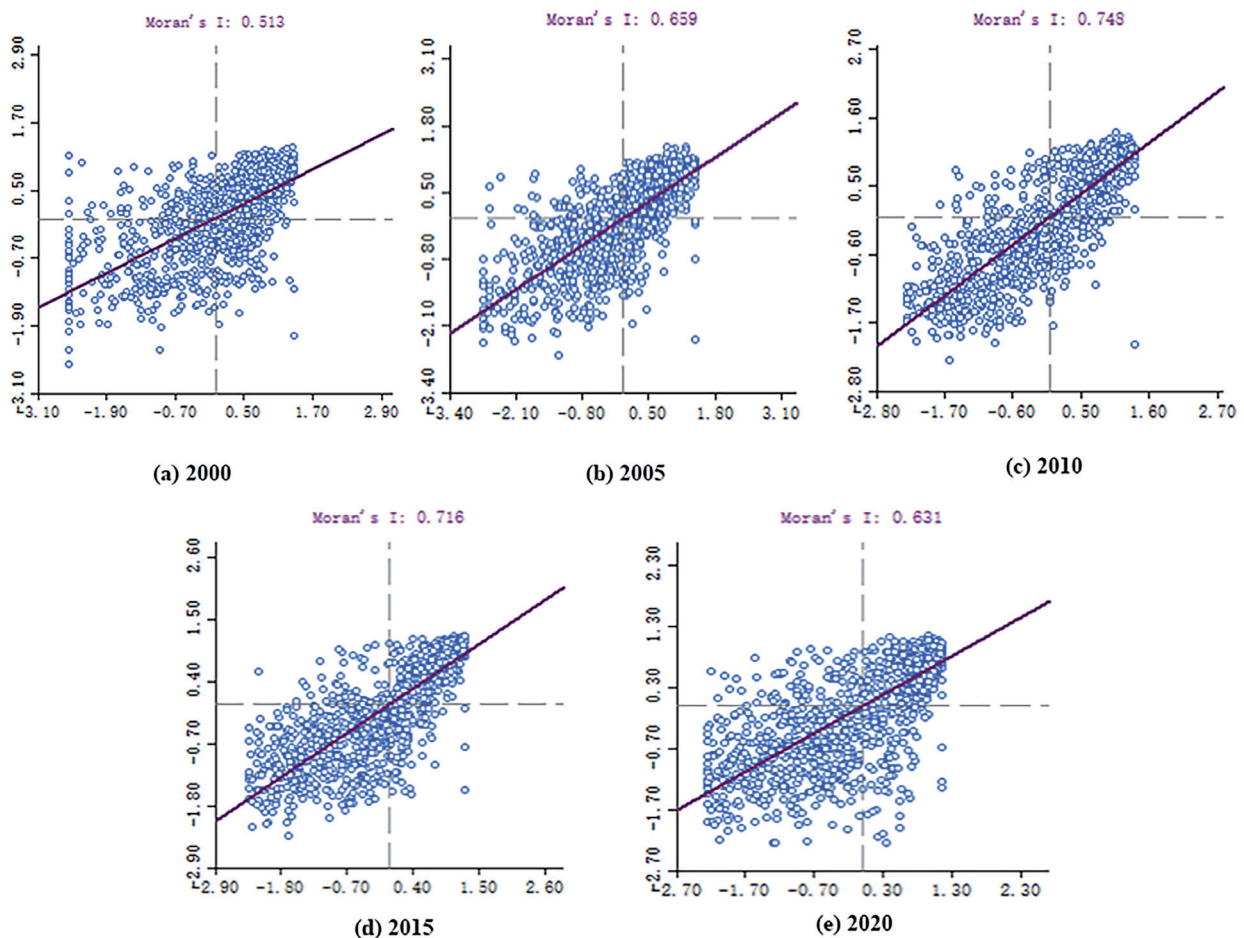


Fig. 4. Moran scatterplot of RSEI during 2000-2020.

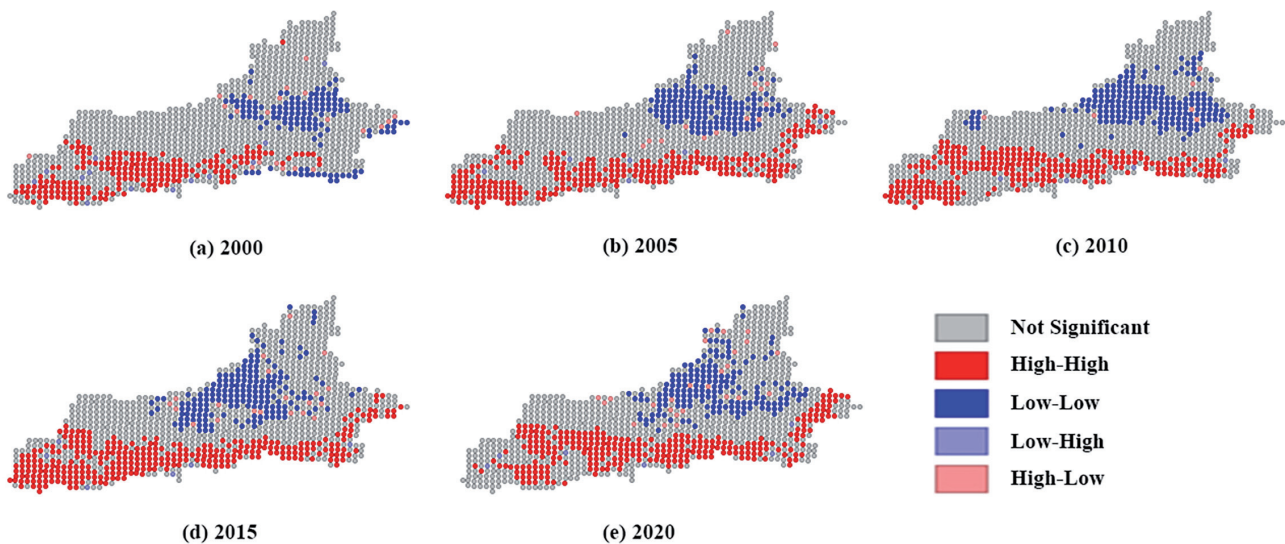


Fig. 5. LISA cluster map of the RSEI in Xi'an.

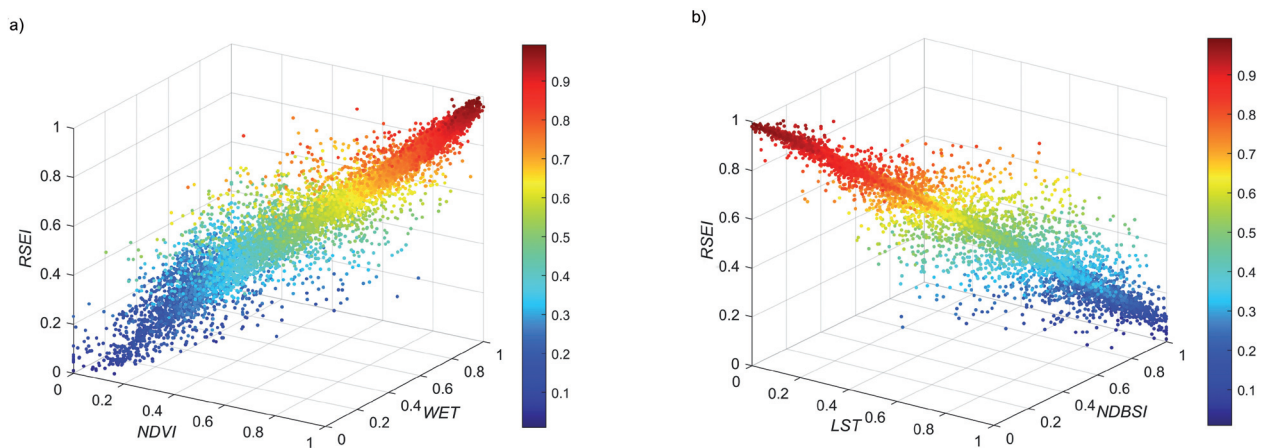


Fig. 6. 3D scatterplots of NDVI, WET, NDBSI, LST, and RSEI of the sampling points.

[63, 64]. This method is intuitive, and can directly identify the different factors with a high or low level of influence through plots [39, 65]. Urban population density, GDP per capita, land-use types, etc. all have significant positive or negative synergistic relationships with RSEI. To further investigate the driving factors of spatial divergence in RSEI, scholars have studied various regions using the geodetector model [56, 57, 66]. There are differences in the extent of the study area due to the various unit scales of the geodetector. Still, the results are informative due to the similarity of the selected driving factors. Generally, the selected driving factors all significantly influence the spatial variation of ecological quality in the 5% interval [57]. And the driving forces of natural factors were generally greater than the driving forces of social factors [58, 59].

Although natural factors play a more pronounced role in the spatial variation of RSEI, the variation of RSEI in a region is mainly influenced by anthropogenic

factors. In the regions after land remediation, the vegetation cover was significantly improved, and the soil moisture increased. This phenomenon was often found in abandoned mining areas and important ecological areas such as coastal zones and ecological reserves. In contrast, in rapid urbanization areas, the RSEI value decreased significantly due to the rapid expansion of the construction land, which triggers the heat island effect and the drying of urban land. As a rapidly urbanizing region, government of Xi'an should pay extreme attention to ecological changes and focus on ecological restoration during urban development.

Validation of LST Inversion Results

In this paper, we used Landsat datasets to obtain the 30 m resolution surface temperatures for 2000, 2005, 2010, 2015, and 2020 in the study area by inversion. The LST result that stands for heat index is a crucial factor

in the analysis of the RSEI model. Therefore, accuracy validation is required. The surface temperature product of MODIS datasets (MOD11A2) has been widely used to measure regional-scale surface temperature characteristics [67, 68]. MOD11A2 data have a spatial resolution of 1 km and a temporal resolution of eight days. We screened the high-quality MOD11A2 data with the same study time in this paper. After we resampled the inversion Landsat surface temperature data to 1 km resolution, we compared them with the corresponding MOD11A2 data. After linear fittings, the inversion results of surface temperature in Xi'an for 2000, 2005, 2010, 2015, and 2020 fit well with the MOD11A2 datasets with the R^2 of 0.70, 0.72, 0.77, 0.79, and 0.80, respectively. The LST results in this paper are in high agreement with the MOD11A2 products and can meet the accuracy requirements.

Geodetector Accuracy Analysis

Different grid sizes influenced the results of geodetector, which can produce scale effects [69]. We chose different sizes of grids of the geodetector for measurement, and the analysis of the results selected the best grid size for the study area. In this paper, 3 km resolution and 5 km resolution grids were chosen for sampling in the research process. The results showed that the main impact factors of the two methods remain unchanged. However, differences emerge in the detection results of impact factors that had a more negligible impact on the ecological quality of the region, which indicated that the accuracy of the geographic detectors was relatively improved the smaller the grid and the more sampling points. Since the dependent variable of the geodetector needs to be discretized, and different discretization methods can lead to different results, this paper compares the results of two methods, quantile grading and natural breakpoint method [48]. In the geodetector model settings, the larger the q-value of the model results, the more reasonable the grading results are implied. Since the natural breakpoint method is based on the natural grouping of data and can maximize the differences between groups, the natural breakpoint method is finally chosen as the grading method in this paper.

Limitations and Future Perspectives

This study evaluated the urban ecological environment quality of Xi'an using the RSEI model based on the Google Earth Engine platform. Through our research, we further explored the spatial variation of urban ecological quality under the influence of natural and social factors. This paper presents an exploration direction for the RSEI model in the quick evaluation of urban ecological environment quality. However, this study has some limitations that need improvement in future research. Firstly, the cloud removal function provided by Google Earth Engine used in this paper

can only mask a small number of clouds in the practical application process. Its effect has been poor for the year with more significant clouds. Secondly, the low resolution of some data in the geodetector affects the q-value of the final result. Thirdly, this paper only selected the greenness, wetness, heat, and dryness indexes to build the RSEI model. Habitat quality, land fragility index, air pollution index, and other reflecting indexes, should be considered in future studies.

Despite the above limitations, the RSEI model based on Google Earth Engine is a fast method that can dynamically monitor the quality of the regional ecological environment. We will use remote sensing data to build the improved RSEI model for cities in different natural and social environments. Further, we will focus on the long-time series of dynamic change characteristics of RSEI and its synergistic relationship with various factors.

Conclusions

In this paper, we used the Google Earth Engine platform to acquire high-quality remote sensing images of Xi'an from July to September 2000, 2005, 2010, 2015, and 2020. We used the cloud removal function provided by the platform to mask the cloud layers. Also, we extracted remote sensing indexes such as greenness, humidity, dryness, and heat to construct the ecological index RSEI using principal component analysis. A geodetector model was used to detect the single factor explanatory power of eight factors and the degree of influence of multifactor interactions, which affect the spatially divergent characteristics of the urban RSEI. The specific conclusions are as follows.

(1) The results of the principal component analysis of the four indicator components of the RSEI model can detail the changes in urban ecological quality in Xi'an. The eigenvectors of the greenness and humidity indicators are positive and have a positive effect on the RSEI. In contrast, the eigenvectors of the heat and dryness indicators are negative and have a negative impact on the RSEI. The greenness and dryness indexes greatly influence the region's RSEI, and the increase in vegetation cover and the decrease of surface dryness are fundamental reasons for the optimization of RSEI.

(2) The ecological environment quality of Xi'an city from 2000 to 2020 showed a temporal trend of decreasing and then increasing, and a spatial trend of mid-low and surround-high. The RSEI value for Xi'an was 0.665 in 2000, 0.653 in 2005, 0.623 in 2010, 0.644 in 2015, and rose to 0.651 in 2020. The RSEI of 2010 was the lowest. The RSEI values in the central built-up area of Xi'an, i.e., the "six urban districts," have significantly decreased. The RSEI values around the settlements in the combined urban-rural areas have also degraded. The area of poor ecological quality in Xi'an increased from 597.20 km² in 2000 to 1081.30 km² in 2020, increasing 81.06%. The area with excellent

ecological quality shows a trend of increasing. In 2020, compared with 2000, the area increased by 986.20 km², and the area of excellent quality was the smallest in 2005, accounting for 34.70%.

(3) Elevation (DEM), slope (SLO), precipitation (PRE), temperature (TEM), distance to main roads (ROA), distance to settlements (SET), land use/land cover (LUC), GDP, and population (POP) significantly influenced the regional RSEI spatial differentiation. The rankings of the explanatory power of the single factors were mainly: PRE>TEM>DEM>ROA>LUC>SLO>GD>SET>POP. All factors showed a bi-enhancement trend under the interaction from the multifactor interaction detection results. PRE has the strongest explanatory power for the spatially divergent characteristics of RSEI. PRE \cap ROA is the highest interaction results.

(4) The RSEI showed significant spatial autocorrelation in Xi'an city. The Global Moran's I was 0.513 in 2000, 0.659 in 2005, 0.749 in 2010, 0.716 in 2015, and 0.631 in 2020, respectively, with the highest value in 2010. From the results of Local Moran's I, the No Significant area was mainly distributed in the rural area around the central city. In contrast, the H-H clustering area was distributed primarily in the northern part of the city, and the L-L clustering area was distributed in the middle and east.

Acknowledgments

This research was funded by the Annual Project of the Social Science Foundation of Shaanxi Province (2020D015), the Key Scientific Research Program of Shaanxi Provincial Education Department (20JT040), and the Soft Science Research Program Project of Xi'an (21RKYJ0053). The authors are thankful for the kind help from Hector Aldrix Santoni Gomez from Xi'an University of Architecture and Technology with English improvement of language, grammar, clarity, and readability of this manuscript.

Conflict of Interest

The authors declare no conflict of interest.

References

1. SOWINSKA-SWIERSKOSZ B. Application of surrogate measures of ecological quality assessment: The introduction of the Indicator of Ecological Landscape Quality (IELQ) [J]. *Ecological Indicators*, **73**, 224, **2017**.
2. LI H., HUANG J., LIANG Y., WANG H., ZHANG Y. Evaluating the quality of ecological environment in Wuhan based on remote sensing ecological index [J]. *Journal of Yunnan University. Natural Science*, **42** (1), 81, **2020**.
3. LIU Z., XU H., LI L., TANG F., LIN Z. Ecological Change in the Hangzhou Area Using the Remote Sensing

- Based Ecological Index [J]. *Journal of Basic Science and Engineering*, **23** (4), 728, **2015**.
4. YANG S., SU H. Multi-Scenario Simulation of Ecosystem Service Values in the Guanzhong Plain Urban Agglomeration, China [J]. *Sustainability*, **14** (14), 8812, **2022**.
5. ZHANG Y., ZHANG K., MAN W., LIU M., HAO Y., HU Y., HU Y., TONG Z. Dynamic research on the ecological environment quality of Shenzhen based on remote sensing indicator [J]. *Environmental Pollution and Control*, **43** (7), 909, **2021**.
6. ZHUANG Q.W., SHAO Z.F., LI D.R., HUANG X., CAI B.W., ALTAN O., WU S.X. Unequal weakening of urbanization and soil salinization on vegetation production capacity [J]. *Geoderma*, **411**, 115712, **2022**.
7. ZHUANG Q.W., SHAO Z.F., HUANG X., ZHANG Y., WU W.F., FENG X.X., LV X.W., DING Q., CAI B.W., ALTAN O. Evolution of soil salinization under the background of landscape patterns in the irrigated northern slopes of Tianshan Mountains, Xinjiang, China [J]. *Catena*, **206**, 10, **2021**.
8. ZHUANG Q.W., WU S.X., HUANG X., KONG L., YAN Y.Y., XIAO H., LI Y.Z., CAI P. Monitoring the impacts of cultivated land quality on crop production capacity in arid regions [J]. *Catena*, **214**, 106263, **2022**.
9. TZOULAS K., KORPELA K., VENN S., YLI-PELKONEN V., KAZMIERCZAK A., NIEMELA J., JAMES P. Promoting ecosystem and human health in urban areas using Green Infrastructure: A literature review [J]. *Landscape and Urban Planning*, **81** (3), 167, **2007**.
10. HUETE A., DIDAN K., MIURA T., RODRIGUEZ E. P., GAO X., FERREIRA L.G. Overview of the radiometric and biophysical performance of the MODIS vegetation indices [J]. *Remote Sensing of Environment*, **83** (1-2), 195, **2002**.
11. JIAPAER G., LIANG S.L., YI Q.X., LIU J.P. Vegetation dynamics and responses to recent climate change in Xinjiang using leaf area index as an indicator [J]. *Ecological Indicators*, **58**, 64, **2015**.
12. WANG X.D., ZHONG X.H., LIU S.Z., LIU J.G., WANG Z.Y., LI M.H. Regional assessment of environmental vulnerability in the Tibetan Plateau: Development and application of a new method [J]. *Journal of Arid Environments*, **72** (10), 1929, **2008**.
13. WAN Z. M., DOZIER J. A generalized split-window algorithm for retrieving land-surface temperature from space [J]. *Ieee Transactions on Geoscience and Remote Sensing*, **34** (4), 892, **1996**.
14. BASNYAT P., TEETER L.D., LOCKABY B.G., FLYNN K.M. The use of remote sensing and GIS in watershed level analyses of non-point source pollution problems [J]. *Forest Ecology and Management*, **128** (1-2), 65, **2000**.
15. BOND T.C., DOHERTY S.J., FAHEY D.W., FORSTER P.M., BERNTSEN T., DEANGELO B.J., FLANNER M.G., GHAN S., KARCHER B., KOCH D., KINNE S., KONDO Y., QUINN P.K., SAROFIM M.C., SCHULTZ M.G., SCHULZ M., VENKATARAMAN C., ZHANG H., ZHANG S., BELLOUIN N., GUTTİKUNDA S.K., HOPKE P.K., JACOBSON M.Z., KAISER J.W., KLIMONT Z., LOHMANN U., SCHWARZ J.P., SHINDELL D., STORELVMO T., WARREN S.G., ZENDER C.S. Bounding the role of black carbon in the climate system: A scientific assessment [J]. *Journal of Geophysical Research-Atmospheres*, **118** (11), 5380, **2013**.
16. SHAN W., JIN X.B., REN J., WANG Y.C., XU Z.G., FAN Y.T., GU Z.M., HONG C.Q., LIN J.H., ZHOU Y.K.

- Ecological environment quality assessment based on remote sensing data for land consolidation [J]. *Journal of Cleaner Production*, **239**, 118126, **2019**.
17. XU H. A remote sensing index for assessment of regional ecological changes [J]. *China Environmental Science*, **33** (5), 889, **2013**.
 18. CUI J., ZHU M.S., MI H.Z., LIU Y.H. Evaluation of Eco-Environmental Quality and Analysis on Spatio-Temporal Variation in Jinan, China [J]. *Polish Journal of Environmental Studies*, **31** (2), 1061, **2022**.
 19. ASCOUGH J.C., MAIER H.R., RAVALICO J.K., STRUDLEY M.W. Future research challenges for incorporation of uncertainty in environmental and ecological decision-making [J]. *Ecological Modelling*, **219** (3-4), 383, **2008**.
 20. SONG H.-M., XUE L. Dynamic monitoring and analysis of ecological environment in Weinan City, Northwest China based on RSEI model [J]. *Yingyong Shengtai Xuebao*, **27** (12), 3913, **2016**.
 21. JIANG C.-L., WU L., LIU D., WANG S.-M. Dynamic monitoring of eco-environmental quality in arid desert area by remote sensing: Taking the Gurbantunggut Desert China as an example [J]. *Yingyong Shengtai Xuebao*, **30** (3), 877, **2019**.
 22. JING Y.Q., ZHANG F., HE Y.F., KUNG H.T., JOHNSON V.C., ARIKENA M. Assessment of spatial and temporal variation of ecological environment quality in Ebinur Lake Wetland National Nature Reserve, Xinjiang, China [J]. *Ecological Indicators*, **110**, 105874, **2020**.
 23. YUAN B.D., FU L.N., ZOU Y., ZHANG S.Q., CHEN X.S., LI F., DENG Z.M., XIE Y.H. Spatiotemporal change detection of ecological quality and the associated affecting factors in Dongting Lake Basin, based on RSEI [J]. *Journal of Cleaner Production*, **302**, 126995, **2021**.
 24. LIU L.-B., XIONG K.-N., REN X.-D. Assessment of Ecological Environment Status in the Longxi-Hongkou National Nature Reserve Based on Remote Sensing Ecological Index [J]. *Journal of Ecology and Rural Environment*, **36** (2), 202, **2020**.
 25. ZHU D.Y., CHEN T., ZHEN N., NIU R.Q. Monitoring the effects of open-pit mining on the eco-environment using a moving window-based remote sensing ecological index [J]. *Environmental Science and Pollution Research*, **27** (13), 15716, **2020**.
 26. SUN C.J., LI X.M., ZHANG W.Q., LI X.G. Evolution of Ecological Security in the Tableland Region of the Chinese Loess Plateau Using a Remote-Sensing-Based Index [J]. *Sustainability*, **12** (8), 3489, **2020**.
 27. GUO K.M., ZHAO J.T., WANG X.Y., XIE Y.W. Spatio-Temporal Dynamics of Environmental Status Based on a Remote Sensing Ecological Distance Index (RSEDI) in the Oases of Hexi Corridor in Northwest China [J]. *Polish Journal of Environmental Studies*, **30** (6), 4997, **2021**.
 28. HU X.S., XU H.Q. A new remote sensing index for assessing the spatial heterogeneity in urban ecological quality: A case from Fuzhou City, China [J]. *Ecological Indicators*, **89**, 11, **2018**.
 29. GORELICK N., HANCHER M., DIXON M., ILYUSHCHENKO S., THAU D., MOORE R. Google Earth Engine: Planetary-scale geospatial analysis for everyone [J]. *Remote Sensing of Environment*, **202**, 18, **2017**.
 30. XIONG Y., XU W.H., LU N., HUANG S.D., WU C., WANG L.G., DAI F., KOU W.L. Assessment of spatial temporal changes of ecological environment quality based on RSEI and GEE: A case study in Erhai Lake Basin, Yunnan province, China [J]. *Ecological Indicators*, **125**, 107518, **2021**.
 31. YANG X.Y., MENG F., FU P.J., ZHANG Y.X., LIU Y.H. Spatiotemporal change and driving factors of the Eco-Environment quality in the Yangtze River Basin from 2001 to 2019 [J]. *Ecological Indicators*, **131**, 108214, **2021**.
 32. ZHANG H., SONG J.-Y., LI M., HAN W.-H. Eco-environmental quality assessment and cause analysis of Qilian Mountain National Park based on GEE [J]. *Shengtaixue Zazhi*, **40** (6), 1883, **2021**.
 33. WANG Y., ZHAO Y., WU J. Dynamic monitoring of long time series of ecological quality in urban agglomerations using Google Earth Engine cloud computing: A case study of the Guangdong-Hong Kong-Macao Greater Bay Area, China [J]. *Acta Ecologica Sinica*, **40** (23), 8461, **2020**.
 34. YAN Y.Y., ZHUANG Q.W., ZAN C.J., REN J., YANG L., WEN Y., ZENG S., ZHANG Q., KONG L. Using the Google Earth Engine to rapidly monitor impacts of geohazards on ecological quality in highly susceptible areas [J]. *Ecological Indicators*, **132**, 108258, **2021**.
 35. YANG Y., LI W.J. The evolution of the ecological footprint and its relationship with the urban development of megacities in Western China: The case of Xi'an [J]. *Journal of Environmental Management*, **243**, 463, **2019**.
 36. YUE H., LIU Y., LI Y., LU Y. Eco-Environmental Quality Assessment in China's 35 Major Cities Based On Remote Sensing Ecological Index [J]. *Ieee Access*, **7**, 51295, **2019**.
 37. ZHU X.M., WANG X.H., YAN D.J., LIU Z., ZHOU Y.F. Analysis of remotely-sensed ecological indexes' influence on urban thermal environment dynamic using an integrated ecological index: a case study of Xi'an, China [J]. *International Journal of Remote Sensing*, **40** (9), 3421, **2019**.
 38. XU H. A Study on Information Extraction of Water Body with the Modified Normalized Difference Water Index (MNDWI) [J]. *Journal of Remote Sensing*, **9** (5), 589, **2005**.
 39. HUANG H.P., CHEN W., ZHANG Y., QIAO L., DU Y.Y. Analysis of ecological quality in Lhasa Metropolitan Area during 1990-2017 based on remote sensing and Google Earth Engine platform [J]. *Journal of Geographical Sciences*, **31** (2), 265, **2021**.
 40. LI F.-L., CHANG Q.-R., SHEN J., LIU J. Dynamic monitoring of ecological environment in loess hilly and gully region of Loess Plateau based on remote sensing: A case study on Fuxian County in Shaanxi Province, Northwest China [J]. *Yingyong Shengtai Xuebao*, **26** (12), 3811, **2015**.
 41. CRIST E.P. A TM Tasseled cap equivalent transformation for reflectance factor data [J]. *Remote Sensing of Environment*, **17** (3), 301, **1985**.
 42. BAIG M.H.A., ZHANG L.F., SHUAI T., TONG Q.X. Derivation of a tasseled cap transformation based on Landsat 8 at-satellite reflectance [J]. *Remote Sensing Letters*, **5** (5), 423, **2014**.
 43. VAN DE GRIEND A., OWE M. On the relationship between thermal emissivity and the normalized difference vegetation index for natural surfaces [J]. *International Journal of Remote Sensing*, **14** (6), 1119, **1993**.
 44. CHATTERJEE R.S., SINGH N., THAPA S., SHARMA D., KUMAR D. Retrieval of land surface temperature (LST) from landsat TM6 and TIRS data by single channel radiative transfer algorithm using satellite and ground-based inputs [J]. *International Journal of Applied Earth Observation and Geoinformation*, **58**, 264, **2017**.

45. WENG Q.H., LU D.S., SCHUBRING J. Estimation of land surface temperature-vegetation abundance relationship for urban heat island studies [J]. *Remote Sensing of Environment*, **89** (4), 467, **2004**.
46. WANG J., XU C. Geodetector: Principle and prospective [J]. *Acta Geographica Sinica*, **72** (1), 116, **2017**.
47. GAO H., ZHANG T., FAN H., JIANG S., HUANG Y. Quantitative Analysis of the Factors Affecting Ecological Environment Quality in Yangling Demonstration Zone Based on Geographical Detector [J]. *Journal of Northwest Forestry University*, **35** (5), 185, **2020**.
48. PARIHA H., ZAN M., ALIMJAN K. Remote sensing evaluation of ecological environment in Urumqi City and analysis of driving factors [J]. *Arid Zone Research*, **38**, 1484, **2021**.
49. YU M.Y., XU Y., LI J.Q., LU X.C., XING H.Q., MA M.L. Geographic Detector-Based Spatiotemporal Variation and Influence Factors Analysis of PM_{2.5} in Shandong, China [J]. *Polish Journal of Environmental Studies*, **30** (1), 463, **2021**.
50. MARTIN D. An assessment of surface and zonal models of population [J]. *International Journal of Geographical Information Systems*, **10** (8), 973, **1996**.
51. SHI H., SHI T.G., LIU Q., WANG Z. Ecological Vulnerability of Tourism Scenic Spots: Based on Remote Sensing Ecological Index [J]. *Polish Journal of Environmental Studies*, **30** (4), 3231, **2021**.
52. BOORI M.S., CHOUDHARY K., PARINGER R., KUPRIYANOV A. Spatiotemporal ecological vulnerability analysis with statistical correlation based on satellite remote sensing in Samara, Russia [J]. *Journal of Environmental Management*, **285**, 13, **2021**.
53. SALEH S.K., AMOUSHAH S., GHOLIPOUR M. Spatiotemporal ecological quality assessment of metropolitan cities: a case study of central Iran [J]. *Environmental Monitoring and Assessment*, **193** (5), 20, **2021**.
54. ZHU L.J., MENG J.J., ZHU L.K. Applying Geodetector to disentangle the contributions of natural and anthropogenic factors to NDVI variations in the middle reaches of the Heihe River Basin [J]. *Ecological Indicators*, **117**, 106545, **2020**.
55. CUI R.H., HAN J.Z., HU Z.Q. Assessment of Spatial Temporal Changes of Ecological Environment Quality: A Case Study in Huaibei City, China [J]. *Land*, **11** (6), 944, **2022**.
56. YIN H.R., CHEN C.N., DONG Q.D., ZHANG P.P., CHEN Q.T., ZHU L.Q. Analysis of Spatial Heterogeneity and Influencing Factors of Ecological Environment Quality in China's North-South Transitional Zone [J]. *International Journal of Environmental Research and Public Health*, **19** (4), 2236, **2022**.
57. ZHOU J.B., LIU W.Q. Monitoring and Evaluation of Eco-Environment Quality Based on Remote Sensing-Based Ecological Index (RSEI) in Taihu Lake Basin, China [J]. *Sustainability*, **14** (9), 5642, **2022**.
58. LIU Q., YANG Z.P., HAN F., SHI H., WANG Z., CHEN X.D. Ecological Environment Assessment in World Natural Heritage Site Based on Remote-Sensing Data. A Case Study from the Bayinbuluke [J]. *Sustainability*, **11** (22), 6385, **2019**.
59. JI J.W., WANG S.X., ZHOU Y., LIU W.L., WANG L.T. Spatiotemporal Change and Landscape Pattern Variation of Eco-Environmental Quality in Jing-Jin-Ji Urban Agglomeration From 2001 to 2015 [J]. *Ieee Access*, **8**, 125534, **2020**.
60. LIU C., YANG M.H., HOU Y.T., ZHAO Y.N., XUE X.Z. Spatiotemporal evolution of island ecological quality under different urban densities: A comparative analysis of Xiamen and Kinmen Islands, southeast China [J]. *Ecological Indicators*, **124**, 107438, **2021**.
61. XU H.Q., WANG M.Y., SHI T.T., GUAN H.D., FANG C.Y., LIN Z.L. Prediction of ecological effects of potential population and impervious surface increases using a remote sensing based ecological index (RSEI) [J]. *Ecological Indicators*, **93**, 730, **2018**.
62. HANG X., LI Y.C., LUO X.C., XU M., HAN X.Z. Assessing the Ecological Quality of Nanjing during Its Urbanization Process by Using Satellite, Meteorological, and Socioeconomic Data [J]. *Journal of Meteorological Research*, **34** (2), 280, **2020**.
63. GAO W.L., ZHANG S.W., RAO X.Y., LIN X., LI R.S. Landsat TM/OLI-Based Ecological and Environmental Quality Survey of Yellow River Basin, Inner Mongolia Section [J]. *Remote Sensing*, **13** (21), 14, **2021**.
64. LI T.-T., MA C., GUO Z.-C. Ecological quality evaluation and influencing factors analysis of Helan Mountain based on RSEI [J]. *Shengtaixue Zazhi*, **40** (4), 1154, **2021**.
65. GAO W.L., ZHANG S.W., RAO X.Y., LIN X., LI R.S. Landsat TM/OLI-Based Ecological and Environmental Quality Survey of Yellow River Basin, Inner Mongolia Section [J]. *Remote Sensing*, **13** (21), 4477, **2021**.
66. LI Y.C., ABBAS Z., CHEN D.Y., ZHU Z.Y., GUO H.J., ZHAO Y.L. The Eco-Environmental Changes in Typical Coastal Zones of Southern China From 1987 to 2020: A Case Study of Guangdong Coastal Counties [J]. *Frontiers in Environmental Science*, **10**, 338, **2022**.
67. HENGL T., HEUVELINK G.B.M., TADIC M.P., PEBESMA E.J. Spatio-temporal prediction of daily temperatures using time-series of MODIS LST images [J]. *Theoretical and Applied Climatology*, **107** (1-2), 265, **2012**.
68. ZHANG G.Q., YAO T.D., XIE H.J., QIN J., YE Q.H., DAI Y.F., GUO R.F. Estimating surface temperature changes of lakes in the Tibetan Plateau using MODIS LST data [J]. *Journal of Geophysical Research-Atmospheres*, **119** (14), 8552, **2014**.
69. SONG Y.Z., WANG J.F., GE Y., XU C.D. An optimal parameters-based geographical detector model enhances geographic characteristics of explanatory variables for spatial heterogeneity analysis: cases with different types of spatial data [J]. *Giscience & Remote Sensing*, **57** (5), 593, **2020**.